Gradient Optimized Gradient-Echo Gradient Moment Nulling Sequences for Flow Compensation of Brain Images

Geon-Ho Jahng[1], Stephen Pickup[2]

Gradient moment nulling techniques require the introduction of an additional gradient on each axis for each order of motion correction to be applied. The additional gradients introduce new constraints on the sequence design and increase the demands on the gradient system. The purpose of this paper is to demonstrate techniques for optimization of gradient echo gradient moment nulling sequences within the constraints of the gradient hardware. Flow compensated pulse sequences were designed and implemented on a clinical magnetic resonance imaging system. The design of the gradient moment nulling sequences requires the solution of a linear system of equations. A Mathematica package was developed that interactively solves the gradient moment nulling problem. The package allows the physicist to specify the desired order of motion compensation and the duration of the gradients in the sequence with different gradient envelopes. The gradient echo sequences with first, second, and third order motion compensation were implemented with minimum echo time. The sequences were optimized to take full advantage of the capabilities of the gradient hardware. The sequences were used to generate images of phantoms and human brains. The optimized sequences were found to have better motion compensation than comparable standard sequences.

Index words : MRI, High order flow compensation, GMN, Gradient envelope

Introduction

Flow artifacts are a subset of general motion artifacts that are caused by blood or cerebrospinal fluid (CSF) flow (1, 2), and these artifacts will differ depending on the flow velocity, direction, and scan parameters. They may be manifest as ghost artifacts, signal dropout, or as flow-specific misregistration (3, 4). Gradient moment nulling (GMN), also known as motion artifact suppression technique (MAST) and gradient motion refocusing (GMR), is the most suitable technique for correction of artifacts due to flow (4).

When designing GMN sequences, it is desirable to keep the sequence as short as possible in order to minimize flow artifacts. However, as the echo time (TE) becomes shorter, so too must the gradient pulses. Simultaneously, the gradient amplitudes must increase

JKSMRM 4:20-26(2000)

[1]Medical Physics in Nuclear Engineering Programs

[2]Department of Radiology University of Missouri-Columbia, Columbia, Missouri 65211, USA

Received; Sept. 29, 1999, acceepted; April 10, 2000

Address reprint requests to : Geon-Ho Jahng, Ph.D., Department of Diagnostic Imaging and Therapeutics BSAC, MC-2017
University of Connecticut Health Center, 263 Farmington Ave. Farmington, CT 06030-2017
Tel. 1-860-679-2614 (Work), 1-860-313-1386(Home), Fax. 1-860-679-1989, Email: jahng@fmri.uchc.edu

in order to keep the gradient integrals constant. As the TE becomes shorter, one eventually reaches the point at which needed gradient amplitudes exceed the capabilities of the system.

A study of the effectiveness of various orders of motion correction showed that there is little benefit from correcting for motion of orders higher than third (5). We are, therefore, interested in solving the GMN problem for up to the third order motion compensation with the constraint of minimal TE. The objective of this paper is to optimize the gradient echo (GE)-GMN sequences by a compact gradient system defined by several different gradient envelopes with several different orders of compensation.

Theory

In this section, we review the spin phase problems that occur in the presence of flow (4, 6, 7) and we must resort to numerical integration techniques as originally proposed by Pattany (4). Flow during an imaging sequence causes a phase error in the moving spins which is a function of the motion and the gradients used in the sequence. The phase error can be expressed in a general form that readily allows for extension to arbitrary orders of motion and gradient pulse envelopes. We begin with the equation for the phase of spins as a function of time

$$\phi(t) = \gamma \int_{t'=0}^{t'=t} r(t')G(t')dt' \qquad [1]$$

where ϕ is the phase of the spins at time t, γ is the gyromagnetic ratio, r(t) is the time dependent position of the spins along the gradient axis, and $G(t)$ is the time dependent gradient amplitude. Here, we have assumed that the spin system is on resonance. The time dependent position of the spins can be expanded as a Taylor series. For the gradient envelopment, if it is assumed that all of the gradient pulses have the same shape and differ only in duration and magnitude, then $G(t) = G\,g(t)$. The phase evolution for the k'th component of motion takes the form

$$\phi_k(t) = \gamma G \int_{t'=0}^{t'=t} \sum_{k=0}^{n} \frac{t^k}{k!} \frac{d^k r}{dt'^k} g\left(\frac{t'-t_s}{t_e-t_s}\right) dt' \qquad [2]$$

where G is a time-independent gradient amplitude, $g(t)$ is the gradient shape function which is defined over the range of 0 to 1, t_s is the time the gradient pulse begins, and te is the time it ends. The summation part is related to the Taylor series.

Under these conditions, the effect of a sequence of gradient pulses may be expressed in matrix form

$$\begin{bmatrix} \int_0^{t_1} g(t,0,t_1)dt & \int_{t_1}^{t_2} g(t,t_1,t_2)dt & \cdots & \int_{t_{m-1}}^{t_m} g(t,t_{m-1},t_m)dt \\ \int_0^{t_1} g(t,0,t_1)t dt & \int_{t_1}^{t_2} g(t,t_1,t_2)t dt & \cdots & \int_{t_{m-1}}^{t_m} g(t,t_{m-1},t_m)t dt \\ \vdots & \vdots & & \\ \int_0^{t_1} g(t,0,t_1)t^n dt & \int_{t_1}^{t_2} g(t,t_1,t_2)t^n dt & \cdots & \int_{t_{m-1}}^{t_m} g(t,t_{m-1},t_m)t^n dt \end{bmatrix} \begin{bmatrix} M_1 \\ M_2 \\ \vdots \\ M_{m-1} \\ M_m \end{bmatrix} = \begin{bmatrix} \phi_0 \\ \phi_1 \\ \vdots \\ \phi_{n-2} \\ \phi_{n-1} \end{bmatrix}$$

$$\mathbf{P} \cdot \mathbf{G} = \mathbf{W} \qquad [3]$$

where m is the number of gradient pulses, n is the truncation order of the Taylor series, M_i is the magnitude of the i'th gradient and ϕ_j is the phase contribution due to the spins having the j'th order of motion. In the above equation, we have introduced the following shorthand notation for compactness

$$g(t,t_e,t_s) = \frac{\gamma}{k!} \frac{d^k r}{dt^k} g\left(\frac{t-t_s}{t_s-t_e}\right) \qquad t_e \le t_s \qquad [4]$$

The gradient magnitudes needed to produce any desired phase vector, $\mathbf{W}$, are readily found by inverting the gradient moment matrix, $\mathbf{P}$, to yield the gradient amplitude vector. In some cases, the requirement that all of the gradient pulses have the same shape is problematic. For example, when using trapezoidal gradient envelopes, it is common practice to set the ramp time for all gradient pulses in a sequence to the same value in order to simplify sequence development. If the gradient pulses do not all have the same total duration, this amounts to a distortion of the pulse shape. For pulses defined in this way, we have found it useful to break each gradient pulse into three parts; the ramp up, the plateau, and the ramp down. The gradient amplitudes are then given by

$$\mathbf{G} = [\mathbf{P}_u + \mathbf{P}_P + \mathbf{P}_d]^{-1} \cdot \mathbf{W} \qquad [5]$$

where the subscripts u, p, and d are used to label the gradient moment matrix for the gradient ramp up, plateau, and ramp down components of the pulses, respectively.

Materials and Methods

For sequence design, the minimum field of view (FOV) and slice thickness (TH) having practical utility in the clinical environment is about 100 mm² and 2mm, respectively. We, therefore, use these values as the limiting threshold for the in-plane gradients in our sequences. A Mathmetica package (Wolfram, 100 Trade Center Drive, Champaign, IL) was used for calculating

gradient duration and amplitudes in the design of flow compensated sequences. Shape functions, $g(t)$, have been defined for pulses with linear or sine ramps. Gradient echo sequences with up to the third order motion compensation on the slice and read axes were optimized. All GE-GMN sequences developed in the present study used a 5.12 msec acquisition time giving 195 Hz/pixel. Quarter-sine lobe gradient ramps were used in all of the sequences developed here in order to minimize eddy-current effects. The ramp time was 0.60 msec in all sequences.

The effectiveness of each of the motion compensated pulse sequences was tested in both phantom and human brain exams. Images obtained by the GMN sequences are compared to those obtained without motion compensation using identical imaging parameters. Images of the phantom were generated with the motion compensation sequences developed in the current study both with and without flow. Both in-plane and through-plane flow axes were examined by suitable adjustment orientation of the imaging plane. All phantom studies were run sequentially, and all scans in these studies were run in single slice mode. A variable speed single-phase electric pump (RMI, Middleton, WI) was used to provide precise control of the flow rate for flow phantom images. The setup for the phantom consisted of a water sink, an electric pump, and a long piece of tubing. The central portion of the tubing was wrapped around a cylindrical form in order to assure a circular flow path in the region of interest. The tubing was constructed of latex and was approximately 30 m long with 4 mm inner diameter. The flow velocity was measured by collecting the return water for a fixed time. Velocity was then calculated using the relation: $v = Q/A$ where v is velocity in cm/sec, Q is the flow rate (V/t) of water through the tube in ml/sec, and A is the cross sectional area of the tube in cm^2. The mean flow velocity was set to 17 cm/sec. The in-vivo human brain studies were run in multi-slice mode with images obtained in sagittal, coronal, and transverse orientations using the optimized third order sequences.

The experiments were performed on the superconducting whole body 1.5 T magnetic resonance imaging (MRI) system (Siemens, Erlangen, Germany). The gradient system is capable of producing gradients of up 25 mT/m with rise times as short as 25 microseconds per mT/m. The standard circularly polarized head coil was used for transmission and detection in the phantom and human studies. Coil tuning and matching were performed automatically for each study. Automatic shimming was also performed prior to all measurements.

Results

1. Optimization of Sequences

1) Motion Correction in the Slice Dimension

In the current analysis, it is first necessary to define the time at which the GMN sequence begins. We begin by assuming that time zero corresponds to the center of the slice select radiofrequency (RF) pulse. We then consider a standard imaging sequence in which slice selection consists of application of a RF pulse in combination with a slice selection gradient. This is then followed by a refocusing gradient. To calculate the time at which to begin the GMN sequence, we first integrate the optimized refocusing gradient. We then integrate the selection gradient backward in time until the integral is equal to that of the refocusing gradient. This is then taken as the point at which all spins are in-phase. The excitation pulse used in all of the GE sequences was a 1.024 msec truncated sinc envelope. In this case, the start time for the sequence was found to be t_0 = 0.092msec. The calculated gradient sequence then begins with an asymmetric gradient pulse that is truncated at time t_0. The remaining gradients are assumed to have the symmetric shape.

The number of gradients used in the sequence is equal to the desired order of motion compensation plus two. The last gradient in the sequence must ramp down before the start of data acquisition. The beginning and end of the gradient sequence are thus fixed. All other gradient switching times are adjustable. These parameters are interactively adjusted and the gradient amplitudes are calculated using our Mathematica package. This process continues until all of the gradients in the sequence approach the specified threshold. When this result is achieved, the resulting gradient sequence is programmed into the imager.

2) Motion Correction in the Read Dimension

The calculation for the readout gradient is analogous to that in the slice select direction. The readout gradient is a time-reversed version of the slice selection gradient. The gradient pulse that is on during data acquisition (the

last one in the sequence) is determined by the acquisition parameters and FOV. We wish to initiate the read gradient sequence as early as possible without interfering with slice selection. The read sequence therefore begins at the beginning of the slice selection ramp down, t_0 = 0.512 msec. All of the gradients have a symmetric shape except the last gradient, which is right truncated at the center of the acquisition window. The start and end of the read gradient sequence are thus determined. All other gradient-switching times are then optimized as described previously.

Motion along the phase encoding direction does not contribute significantly to phase artifacts because of the relatively short duration of the phase encoding gradient and its close proximity to the acquisition gradient. The low average amplitude of the phase encoding gradient also minimizes the effects of motion. Motion correction techniques were, therefore, not applied in the phase encode direction (8).

It is generally found that the minimal echo time is limited by the read gradient while the demands on the slice gradient are nominal. It is, therefore, often possible to implement higher order motion compensation on the slice axis than on the read for a given TE. This approach was employed in many of our sequences.

3) Optimized Sequence

The optimized third order GE-GMN sequence is depicted in the Fig. 1. A total of five gradients are applied in both the slice selection and readout directions. The TE in this sequence is 23 msec. In contrast to most pulse sequence diagrams, the gradient amplitudes on a given axis are drawn to scale in the figure. The minimal TE for this sequence is limited by the readout gradient. The magnitude of the last gradient on the read axis is determined by the imaging parameters. Switching times for the remaining gradients were adjusted so that they have nearly the same amplitude, making this sequence very well optimized. The two gradients at the end of the sequence on the slice and phase axes are crushers that eliminate residual magnetization. The data acquisition gradient is also extended beyond the acquisition window for additional suppression of residual magnetization. Minimum FOV and minimum TH are approximately 95 mm and 2 mm, respectively. This limit is suitable for general applications. The time intervals used for the third order sequence, calculated by our Mathmetica tool, are listed in Table1, along with start times for all gradients. The gradient end time for a given gradient is identical to the start time for the next gradient on the same axis.

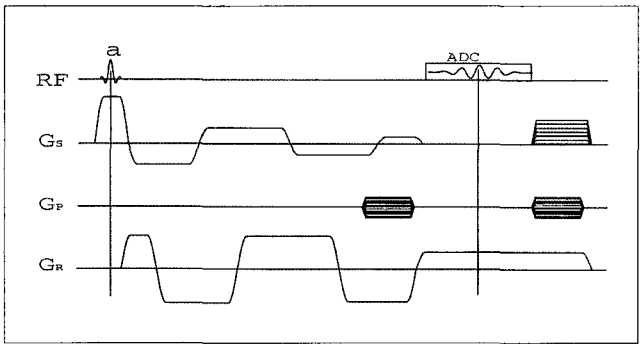

Fig. 1. The GE-GMN sequence with third order motion compensation in the slice and read dimensions is depicted. α is a flip angle(FA). Note that the phase encode gradient was moved to the end of the sequence and crusher gradients are applied at the end.

The first and second order flow compensated sequences were also developed using the methods described above. Sequences with higher order correction on the slice axis were developed when feasible. Several variations of the sequences described here were also developed. Those sequences represent the minimum for the FOV restrictions described previously. All of the motion compensated GE sequences developed in the present study are summarized in Table 2. In the table, the symbols #/S and #/R indicate the order of motion correction on the slice and read axes, respectively, where # is the order of the motion correction.

2. Image Results

1) Phantom Studies

We examined the effectiveness of the first, second, and third order motion compensated GE-GMN sequences (Table 2). In all of the GE images, some suscep-

Table 1. The switching times and amplitudes for the gradient sequence used in the optimized third order GE-GMN sequence calculated by our Mathemetica tool.

G_s		G_r	
t_s (msec)	G (mT/m)	t_s (msec)	G (mT/m)
0.092	4.800000	0.512	4.598633
1.112	-2.143258	2.807	-4.718381
5.702	1.645526	8.086	4.556379
11.669	-1.117512	14.741	-4.543432
17.406	0.736334	19.790	2.354000
20.390		22.950	

tibility artifacts are apparent at the container interface because of relatively long echo time. Air bubbles between the tubing and its support resulted in similar artifacts in that region.

In Figure 2, the third order motion compensated sequence (GE_N33_23) is compared to the standard GE sequence with similar parameters. The imaging parameters used in this study were the repetition time (TR) = 700 msec, TE = 23 msec, TH = 10 mm, FA = 60°, and FOV = 100 mm. The images on the left were acquired using the uncompensated GE sequence. Flow artifacts are clearly evident in both the in-plane (a) and through-plane (c) orientations. Application of the motion correction sequence recovers most of the intensity that was lost due to flow. Note that the flowing fluid has an enhanced intensity in the image relative to the stationary fluid in the motion compensated images. This is due to the fact that the TR in this sequence does not allow the spins to fully recover between repetitions of the sequence. Although the image quality is clearly better in the compensated images, there are some misregistration artifacts present in the in-plane image (b).

Table 2. Summary of GE-GMN sequences developed in the present study.

Sequence Name	Correction order	Minimum TE (msec)	Minimum TR (msec)	Minimum FOV(mm²)	Minimum TH (mm)
GE_N11_10	1/S, 1/R	10	23	86	2
GE_N12_10	2/S, 1/R	10	23	86	2
GE_N22_16	2/S, 2/R	16	29	87	2
GE_N23_16	3/S, 2/R	16	29	87	2
GE_N33_23	3/S, 3/R	23	35	95	2
GE_N33_27	3/S, 3/R	27	38	70	2

Similar exams performed with the other GE-GMN sequences listed in Table 2 yielded comparable results. The signal drop-out in the images generated by the uncompensated sequence is even greater than in the lower order studies. The advantages of high order motion compensation are largely offset by the increased echo time and some signal dropout persists. The shorter echo

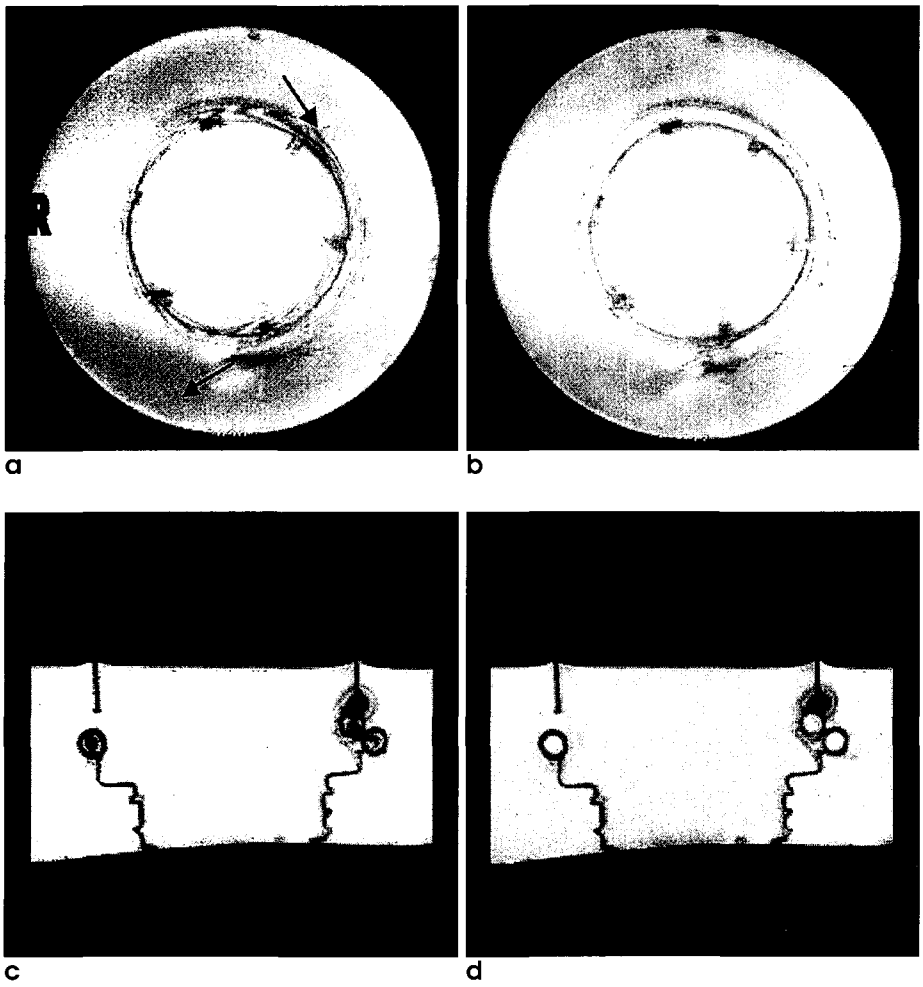

Fig. 2. Images of the flow phantom generated with identical parameters by the simple GE sequence (**a, c**) and third order GE-GMN sequence (**b, d**) are compared. The flow direction is indicated by arrow. TR = 700msec and TE = 23 msec, TH = 10mm, FA = 60°, and FOV = 100mm. *R* is right side. Note that flow artifacts are clearly evident in both the in-plane (**a**) and through-plane (**c**) orientations, but not in (**b**) and (**d**). In through-plane image the dark signal in right-hand side is related to air bubble.

times provided by the low order motion compensation sequences minimizes the flow artifact. As a result, the low order sequences generally performed better than the high order sequences at high flow rates.

2) Human Brain Studies

The third order motion compensated GE-GMN sequence was also evaluated in a clinical setting. Brain images of healthy volunteers were acquired using the new sequence and the uncompensated GE sequence with identical parameters, TR = 700 msec, TE = 23 msec, TH = 10 cm, FA = 60°Δ, and FOV = 200 mm. The results of this analysis (GE_N33_23) are presented in Figure 3. Outer volume suppression techniques were used to suppress any signal that fell outside of the FOV.

Flow artifacts in the form of signal drop-out in the vasculature are clearly evident in the uncompensated images (a, c). Much of this signal is recovered in the motion compensated images (b, d), but a misregistration of the large vasculature is clearly evident. When the vessel lies within the imaging plane this misregistration takes the form of a bright white line of approximately uniform width offset slightly from the true anatomic location of the vessel (6). The GMN images generally showed increased contrast and sharpness compared with standard GE images for studies with long echo times.

Conclusions and Discussion

To reduce the signal loss caused by flowing spins, the GMN technique is used to bring both flowing and stationary spins back to zero phase. Simple additional gradient pulses in commercial sequence are applied with a long linear ramp time and rectangular gradient. This has the disadvantage of leading to problems with eddy currents. In commercial sequences, the first order of flow compensation scheme is sometimes used in long TE. Increasing TE with GMN is a problem compared to real short TE without GMN. Therefore, it is required to make TE as short as possible. Most previously devel-

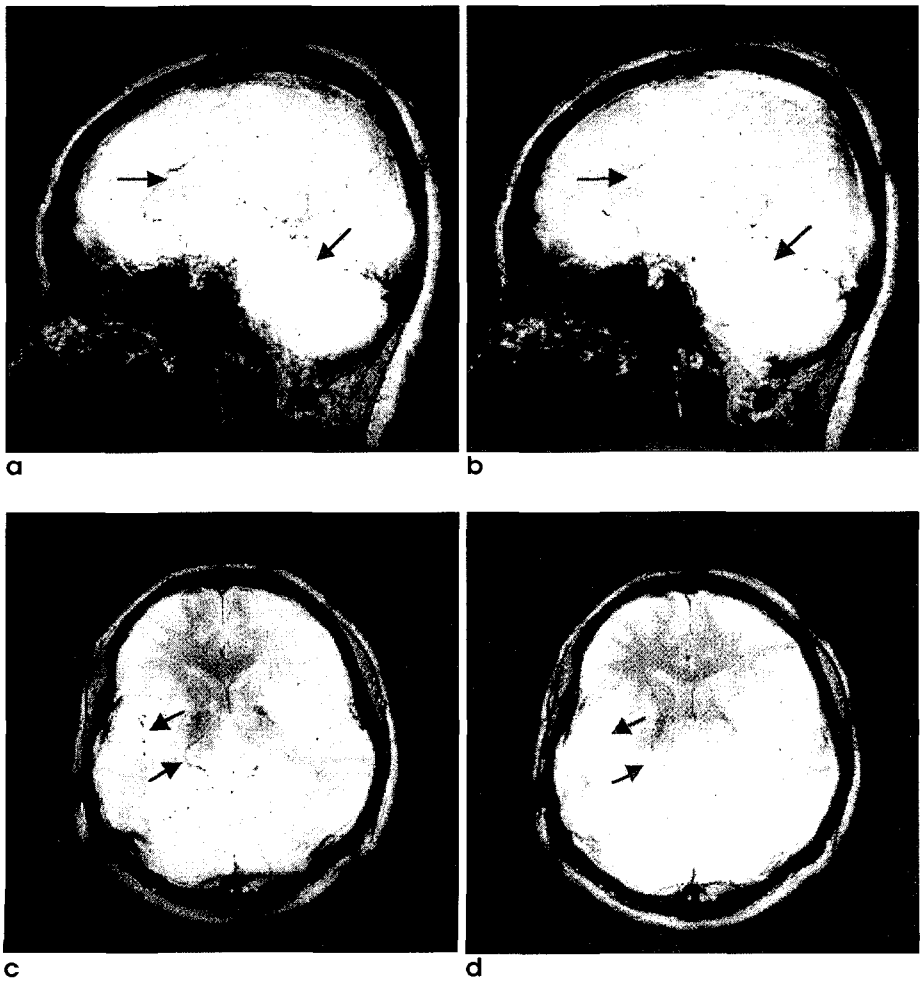

Fig. 3. Human brain images generated by the simple GE (**a, c**) and the third order GE-GMN sequence (**b, d**) are compared. TR = 700msec, TE = 23msec, TH = 10cm, FA = 60°, and FOV = 200mm. Flow artifacts in the form of signal drop-out in the vasculature are clearly evident in the uncompensated images (**a, c**). Two sets of images are easily compared in arrow sits. Much of this signal is recovered in the motion compensated images (**b, d**)

oped GMN techniques were also applied to the same order of flow compensation in any direction or flow compensation in just one direction. With the same TE, it is important to apply higher order of flow compensation within the limitations of FOV, slice thickness, and instrument capabilities(maximum amplitude of gradient and slew rate).

Several motion compensated GE sequences were designed and implemented in the present study. The GMN motion compensation technique is relatively demanding on the gradient hardware (9). It was, therefore, necessary to make optimum use of the limited capabilities of the gradient system. This was achieved by adjusting the gradient timing parameters such that the most intense gradient pulses had approximately the same intensity. If any one gradient in the sequence has substantially larger gradient amplitude than the others, the minimum FOV that the sequence can achieve is limited by that gradient.

Interactive design of GMN sequences was facilitated by development of a Mathematica package that determines the gradient amplitudes given the gradient shape functions and timing parameters. The package is also capable of generating plots of the calculated gradient envelopes and the phase evolution during the gradient sequence. Each of the sequences developed was implemented with the minimum TE for the desired motion compensation order (10). This minimum TE is dictated by the capabilities of the gradient system and the minimum desired FOV. Higher than the third order motion correction was not considered because the increases in TE needed to fit the additional gradients resulted in motion artifacts that could not be corrected by the higher order sequences.

The quality of the motion compensation provided by the sequences developed in the present study was determined by application of the sequences in both flow phantom and human studies. The new sequences were found to have superior motion correction properties and were capable of viewing a smaller FOV than the standard sequences. One advantage of our techniques is that any orders of compensation can be applied with any type of gradient pulse shape, such as a trapezoidal gradient with linear and quarter sine ramp or pure sine gradient. Also, we separately calculated each part of the gradient of the ramp and plateau which gives a more accurate calculations of phase dephasing problems. A quarter sine ramp serves to reduce the limitations of usability imposed by slew rate. An additional advantage is that we used a higher order of motion compensation in slice selection direction than readout encoding direction without increasing TE. This provides better performance in through plane images than the same order compensation in both axes. The GMN technique is limited by the maximum gradient amplitude and slew rate of the gradient system. The only significant disadvantage of GMN seems to be the added stress it places on gradient power supplies.

References

1. Stahlberg F, Mogelvang J, Thomsen C, A Method for MR quantification of flow velocities in blood and CSF using interleaved gradient-echo pulse sequences. Magn Reson Imag 7, 655-667 (1989)
2. Cho MH, Kim WS, Cho ZH, CSF flow artifact reduction using cardiac cycle ordered phase-encoding method. Magn Reson Imag 8, 395-405 (1990)
3. Ehman RL, Felmlee JP, Adaptive technique for high-definition MR imaging of moving structures. Radiology 173, 255-263 (1989)
4. Pattany PM, Phillips JJ, Chiu LC, Motion artifact suppression technique (MAST) for MR imaging. J Computer Assisted Tomography 11 (3), 369-377 (1987)
5. Hinks RS, Constable RT, Gradient moment nulling in fast spin echo. Magn Reson Med 32, 698-706 (1994)
6. Duerk JL, Smonetti OP, Hurst GC, Multiecho multimoment refocusing of motion in magnetic resonance imaging: MEMMO-RE. Magn Reson Imaging 8, 535-541 (1990)
7. Duerk JL, Pattany PM, Analysis of imaging axes significance in motion artifact suppression technique (MAST-TM): MRI of turbulent flow and motion. Magn Reson Imaging 7, 251-263 (1989)
8. Parikh AM, Magnetic resonance imaging techniques, chapter 15, 21, 22, 30, and 34, Elsevier, 1991
9. Pipe JG, Chenenert TL, A progressive gradient moment nulling design technique. Magn Reson Med 19, 175-179 (1991)
10. Bernstein MA, Shimakawa A, Pelc NJ, Minimizing TE in moment-nulled or flow-encoded two- and three-dimensional gradient-echo imaging. J Magn Reson Imag 2 (5), 583-588 (1992)